

# Collective motion of cells crawling on a substrate: roles of cell shape and contact inhibition

Simon K. Schnyder,\* Yuki Tanaka, John J. Molina, and Ryoichi Yamamoto  
*Department of Chemical Engineering, Kyoto University, Kyoto 615-8510, Japan*  
(Dated: March 2, 2022)

Contact inhibition plays a crucial role in the motility of cells, the process of wound healing, and the formation of tumors. By mimicking the mechanical motion of cells crawling on a substrate using a pseudopod, we constructed a minimal model for migrating cells which gives rise to contact inhibition of locomotion (CIL) naturally. The model cell consists of two disks, one in the front (a pseudopod) and the other one in the back (cell body), connected by a finitely extensible spring. Despite the simplicity of the model, the cells' collective behavior is highly nontrivial, depending on the shape of cells and whether CIL is enabled or not. Cells with a small front circle (i.e. a narrow pseudopod) form immobile colonies. In contrast, cells with a large front circle (i.e. such as a lamellipodium) exhibit coherent migration without any explicit alignment mechanism being present in the model. This suggests that crawling cells often exhibit broad fronts because it helps them avoid clustering. Upon increasing the density, the cells develop density waves which propagate against the direction of cell migration and finally arrest at higher densities.

PACS numbers: 87.17.Jj, 87.23.Cc, 87.18.Fx, 05.10.a

Directional collective motion of cells is of fundamental importance for embryogenesis, wound healing and tumor invasion [1–3]. Cells move in clusters, strands or sheets to cover empty area [4], to grow or invade tissues. But how the cells coordinate and control their motion, is the subject of ongoing research. At the level of a single cell, it is well established that its motion is intricately linked to its shape. The shape of crawling cells is highly variable, depending on the type of cell, the substrate, as well as a result of the migration process itself [5–8]. When a cell starts moving, its shape breaks symmetry [6], whereas circular cells typically cannot move. While there is evidence that shape has a strong influence on scattering and can lead to clustering and collective directed motion of swimmers [9, 10], less is known about the role of cell shape in organizing collective crawling. It has been shown in simulations that inelastic collisions between crawling cells, e.g. due to deformation, can lead to coherent migration [11–14], suggesting the importance of deformability for collective behavior. When crawling cells come into contact, it inhibits their protrusions, which tends to change their shape and reorient them [15]. It was shown that this effect called contact inhibition of locomotion (CIL) enables cells to follow chemical gradients more effectively by aligning them [16, 17]. In growing colonies, CIL leads to a slowing down of the motility of individual cells when the density of their environment crosses a certain threshold [18]. CIL thus is believed to play a crucial role in the control of collective tissue migration [12, 16, 19, 20], tissue growth [18, 21], morphogenesis, wound healing and in tumors [22].

Clearly, CIL, cell shape and deformability are linked [12]. Therefore, we built a minimal, mechanical model of cells crawling on a substrate, aiming to isolate behavior purely caused by the interplay of contact inhibition and deformable shape, while neglecting other properties such as cell-cell adhesion and chemotaxis. The simplicity of our model enables us to simulate considerably larger systems as compared to more complex models, which minimizes finite size effects. The

model is based on the accepted picture for a cell crawling on a surface [23–25]: Before it begins migrating, the cell polarizes itself, i.e. front and back become distinguishable. The migration cycle then starts with the cell extending protrusions such as a pseudopod in the direction of motion. Actin polymerization inside the cell is used to drive these protrusions outward. The protrusions adhere to the substrate with adhesion sites, over which the cell exerts traction forces on the substrate. Adhesion sites at the back of the cell are released and then pulled in as the actin cytoskeleton depolymerizes.

In our model, cells are represented by two disks, connected by a finitely extensible string. The cell migrates by periodically contracting and expanding the spring and alternately attaching the disks to the substrate. We speculate on a simple mechanism for contact inhibition where the cell motility is proportional to the extension of the cell, motivated by the observation that cell speed depends on the extension of pseudopods [26]. An alternative motility term where the force is always constant was used for comparison. We find that the average speed of the cells decreases strongly with cell density, an effect that vanishes when we switch contact inhibition off. Further, we find a dynamic phase transition as a function of cell shape: When the front disk is smaller than the back, the cells form colonies. When the front is larger than the back – which is typical for many migrating cells such as keratocytes or fibroblasts [27] – the cells exhibit coherent migration, even though there is no explicit alignment mechanism included in the model. This suggests that the broad front of crawling cells helps those cells avoid clustering. When contact inhibition is switched off, we find weakened alignment, pointing to the relevance of CIL in the collective migration of cells. In the collective-migration state an additional transition is driven by the density of cells. Systems at very high densities completely arrest. Before full arrest the system exhibits strong density fluctuations, where dense regions of arrest travel against the average direction of motion of the cells.

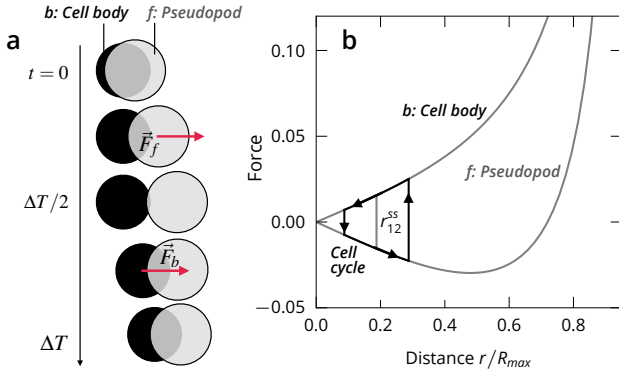


Figure 1. (a) The cell migration cycle which underlies our coarse-grained mechanics. (b) The forces acting in a single cell on the two disks being at distance  $r$ . The two-phase cell migration cycle of (a) is marked as a black path. In the limit of vanishing cycle period, the cell obtains constant extension  $r_{bf}^{ss}$  where the forces exactly balance (marked by grey line).

*Simulation* Each cell consists of a cell body and a pseudopod, modelled as disks with indices  $b$  (back) and  $f$  (front), respectively, see fig. 1(a). Each cell is able to extend and contract itself, and it is able to attach to the substrate with both disks independently. The disks experience a drag force with the substrate  $-\zeta_i \vec{v}_i$  with friction coefficient  $\zeta_i$  and  $\vec{v}_i$  being the velocity of disk  $i$ . We set  $\zeta = \zeta_b = \zeta_f$ . Assuming that substrate friction is large compared to both cell-cell friction and intracellular friction, we neglect the latter two in our model. The crawling mechanism is first modelled in two stages that are repeated cyclically with a time period  $\Delta T$ , see fig. 1(a), and then we perform the limit of  $\Delta T \rightarrow 0$  resulting in continuous motion of the cell. In the first stage of the cell motion, the cell body disk is fixed in place, while the pseudopod is driven forward by an internal force  $\vec{F}_f(t)$  representing the cytoskeleton. For times  $\Delta T/2 < t < \Delta T$ , the cell is in the second stage in which the pseudopod fixes itself and the cell body is drawn in with a contraction force  $F_b(t)$ . In the limit  $\Delta T \rightarrow 0$ , alternated application of each force is replaced by the application of both forces at the same time, with half the magnitude. This can be seen as the assumption that in a real cell, contraction, expansion, as well as fixing and unfixing of body and pseudopod happen at the same time or in close succession. We drop the factor 1/2 coming in from the limit, absorbing it into the definitions of the forces. We model the cytoskeleton as a finitely extensible nonlinear elastic (FENE) spring [28] with an additional linear term  $F_{\text{mig}}$  that can be interpreted as a migration force

$$\begin{aligned} \vec{F}_b(\vec{r}_{bf}) &= \vec{F}_{\text{fene}}(\vec{r}_{bf}) \\ \vec{F}_f(\vec{r}_{bf}) &= -\vec{F}_{\text{fene}}(\vec{r}_{bf}) + \vec{F}_{\text{mig}}(\vec{r}_{bf}), \end{aligned} \quad (1)$$

for the two disks being at distance  $\vec{r}_{bf}$ , with

$$\vec{F}_{\text{fene}}(\vec{r}) = \frac{\kappa \vec{r}}{1 - (r/R_{\text{max}})^2}, \quad \vec{F}_{\text{mig}}(\vec{r}) = m \vec{r} \quad (2)$$

and coupling parameters  $\kappa$ ,  $m$ , see fig. 1.  $R_{\text{max}}$  sets the characteristic length scale. There is no random component to the model, which is a valid assumption when the dynamics are dominated by collisions [29, 30]. This can be expected to hold in particular at intermediate and high cell densities. The cell is only motile when its disks have some separation,  $r_{bf} > 0$ , and thus when its shape deviates from a circle. This kind of coupling of motility and deformation is typical in migratory cells [31]. The migration term  $F_{\text{mig}}$  models contact inhibition, since cells compressed due to contact with their neighbors exert a lowered motility force.

The interaction between disks of different cells is modelled with the short-ranged Weeks-Chandler-Andersen potential [32], since interactions occur mainly via direct contact. All back disks have diameter  $\sigma_b$ , all front disks have diameter  $\sigma_f$ . To allow for different cell shapes,  $\sigma_b$  and  $\sigma_f$  can be different. For the interaction of a pair of disks  $\alpha$  and  $\beta$  ( $\alpha, \beta \in [b, f]$ ) of two different cells at distance  $\vec{r}$ , the interaction diameter is given by  $\sigma_{\alpha\beta} = (\sigma_\alpha + \sigma_\beta)/2$ , the energy scale is given by  $\varepsilon$ , and the force by

$$\vec{F}_{\text{LJ}}(r) = \begin{cases} -24\varepsilon \left[ \left( \frac{2\sigma_{\alpha\beta}}{r} \right)^{12} - \left( \frac{\sigma_{\alpha\beta}}{r} \right)^6 \right] \vec{r}/r^2, & r < r_{\text{cut}}, \\ 0, & r \geq r_{\text{cut}}. \end{cases} \quad (3)$$

The cutoff at  $r_{\text{cut}}^* = 2^{1/6} \sigma_{\alpha\beta}$  makes the inter-cellular forces purely repulsive.

For each of the cells we now have two coupled equations of motion, assuming overdamped dynamics,

$$\begin{aligned} \frac{d}{dt} \vec{r}_b &= \frac{1}{\zeta} \left( \frac{\kappa \vec{r}_{bf}}{1 - (r_{bf}/R_{\text{max}})^2} + \sum_{\text{neigh.}} \vec{F}_{\text{LJ}} \right) \\ \frac{d}{dt} \vec{r}_f &= \frac{1}{\zeta} \left( m \vec{r}_{bf} - \frac{\kappa \vec{r}_{bf}}{1 - (r_{bf}/R_{\text{max}})^2} + \sum_{\text{neigh.}} \vec{F}_{\text{LJ}} \right). \end{aligned} \quad (4)$$

To allow for cell migration, we have to require that  $v_{bf} > 0$  when  $r_{bf} > 0$  for a solitary cell, or otherwise cells would eventually stop migrating by themselves,

$$\frac{d}{dt} \vec{r}_{bf} = \frac{d}{dt} \vec{r}_f - \frac{d}{dt} \vec{r}_b = \frac{1}{\zeta} (m - 2\kappa) \vec{r}_{bf} + \mathcal{O}(r_{bf}^2) > 0.$$

This implies  $m > 2\kappa$ . We chose  $\kappa = 32\varepsilon/R_{\text{max}}^2$  and  $m = 66.3\varepsilon/R_{\text{max}}^2$ , such that  $m = 2.07\kappa$ . At long times, the cell enters a steady state with constant extension  $r_{bf}^{ss}$  in which the forces acting on the cell balance,

$$0 = \frac{d}{dt} \vec{r}_{bf} = \frac{1}{\zeta} \left( m \vec{r}_{bf}^{ss} - \frac{2\kappa r_{bf}^{ss}}{1 - (r_{bf}^{ss}/R_{\text{max}})^2} \right).$$

Thus, steady-state distance  $r_{bf}^{ss}$  and the corresponding cell velocity  $v^{ss}$  are given by

$$\begin{aligned} r_{bf}^{ss} &= R_{\text{max}} \sqrt{1 - 2\kappa/m}, \\ v^{ss} &= \frac{\kappa r_{bf}^{ss}}{\zeta (1 - [r_{bf}^{ss}/R_{\text{max}}]^2)} = r_{bf}^{ss} \frac{m}{2\zeta}. \end{aligned} \quad (5)$$

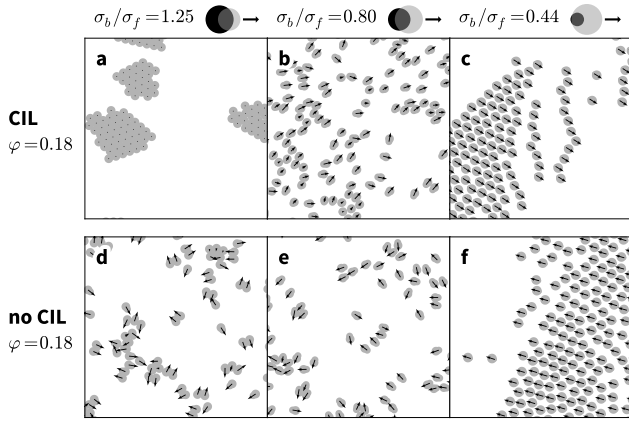


Figure 2. Sections of simulation snapshots of CIL and no-CIL cells for a range of cell shapes with  $\sigma_b/\sigma_f$  as given in the titles. The velocity of cells is given as arrows. (For videos, see supplementary materials)

Then,  $\tau_{\text{mig}} = R_{\text{max}}/v^{\text{ss}} = 2\zeta/(\sqrt{m^2 - 2m\kappa})$  sets the characteristic time scale of migration as the time it takes for a solitary cell in the steady state to travel roughly its own diameter.

For comparison, we use a version of the model without CIL. Replacing the migration force term  $mr_{bf}$  with constant value  $mr_{bf}^{\text{ss}}$  leaves  $r_{bf}^{\text{ss}}$  and  $v^{\text{ss}}$  unchanged, but leads to cells always exerting exactly the same migration force, regardless of whether the local environment allows for extension of the cell. This makes the system more similar to Vicsek-type models with constant speed [33–35].

Cells are placed on random positions in a square simulation box with periodic boundary conditions at area fraction  $\phi$ . The area fraction  $\phi = AN/L^2$  is obtained from the total number of cells  $N$  in the system, the simulation box size  $L$  and the area of a single cell in its steady state  $A \approx 0.288R_{\text{max}}^2$ . Configurations at very large  $\phi$  were obtained by simulating a system of initially lower area fraction for some time and randomly letting individual cells divide into two new cells if there was enough space. We simulated systems with up to  $10^5$  cells to make sure that no finite size effects are present. We integrated the equations of motion until the steady-state was reached. All results are averaged over 10 independent runs with changed starting configurations for the cells.

**Results** In order to investigate the influence of the cell shape on their dynamics, we varied the diameters  $\sigma_b$  and  $\sigma_f$  of the cell disks while keeping the area of the cell in the steady state constant. When the back disk is bigger than the front,  $\sigma_b > \sigma_f$ , the cells tend to form mostly immobile colonies, see fig. 2a). When the front disk is larger than the back,  $\sigma_b < \sigma_f$ , the cell exhibit coherent migration, see fig. 2b). If the front is much larger than the back, the cells completely align and form dense, travelling bands, see fig. 2c). This behavior is quite similar to that of migrating neural crest cells [17, 36] and occurs here without requiring cell-cell attraction. Switching contact inhibition off destroys the ability to form colonies, and leads to weaker alignment at  $\sigma_b/\sigma_f = 0.80$ .

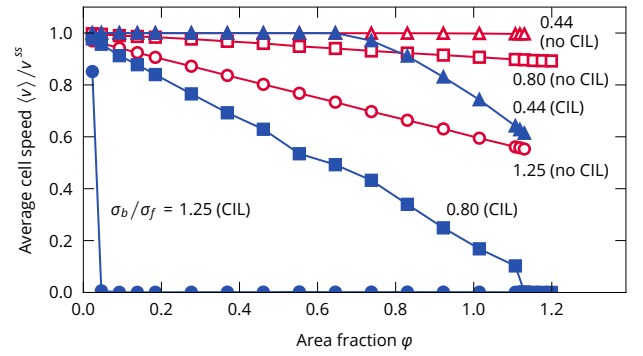


Figure 3. Average speed of the cells in the steady state, normalized by the steady state speed of a solitary cell  $v^{\text{ss}}$ , as a function of area fraction, with (closed symbols) and without contact inhibition (open symbols) and a range of cell shapes.

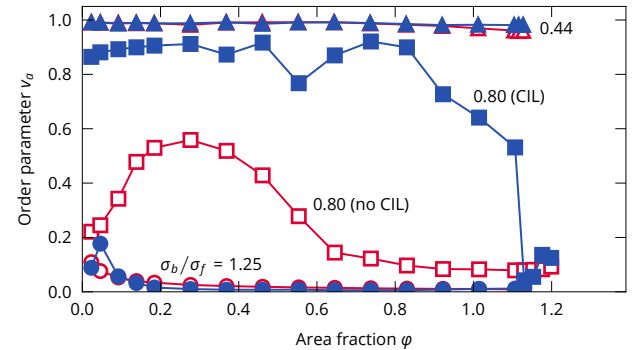


Figure 4. Order parameter  $v_a$  for the same data sets as fig. 3.

Migrating cells exhibiting contact inhibition slow down strongly at high cell densities [18]. To test this in the model, we measured the average cell speed while varying the area fraction of the cells at three shape anisotropies  $\sigma_b/\sigma_f = 1.25$ , 0.80 (the inverse case), and 0.44, see fig. 3. For  $\sigma_b/\sigma_f = 1.25$ , the cell speed vanishes for all but the smallest density due to formation of colonies. In the reverse case,  $\sigma_b/\sigma_f = 0.80$ , the contact inhibited cells crawl at maximum speed only at very small density, with the speed decreasing linearly over nearly the whole density range. The cells fully arrest when they are close-packed, at  $\phi \approx 1.1$  (Area fractions can be larger than 1 because the disks are soft, and because the area fraction has to be defined with the cell's biggest possible area, that of the steady state). At shape anisotropy  $\sigma_b/\sigma_f = 0.44$ , cells are able to crawl at maximum speed up to area fraction  $\phi \approx 0.6$  before a slowing down finally occurs. In comparison, the non-contact-inhibited cells at corresponding anisotropies show a much weaker response to increasing density.

The different response to density is connected to the alignment that the cells are able to achieve. To understand this, we

calculated an order parameter of collective alignment  $v_a$

$$v_a = \frac{1}{N} \left| \sum_{i=1}^N \frac{\vec{r}_{i,f} - \vec{r}_{i,b}}{|\vec{r}_{i,f} - \vec{r}_{i,b}|} \right|, \quad (6)$$

which evaluates to 1 for full alignment of the cell orientations and to 0 for fully random or isotropic orientations, see fig. 4. When the CIL cells cluster into colonies, e.g. at  $\sigma_b/\sigma_f = 1.25$ , the order parameter vanishes, since the orientations of the cells, mostly pointing towards their cluster's center, cancel out. This in turn also leads to vanishing average speed. At  $\sigma_b/\sigma_f = 0.80$ , the cells are mostly aligned for most densities. Alignment weakens in the approach to full arrest. At  $\sigma_b/\sigma_f = 0.44$  the cells are completely aligned at all densities. So for all densities where it is possible for the cells to be spaced far enough from each other so as not to interact (for roughly  $\varphi \leq 0.65$ ) there are little to no collisions and the cells crawl at full speed. When alignment is not perfect, as for  $\sigma_b/\sigma_f = 0.80$ , this is not possible and frequent collisions lower the average speed of the coherently moving cells.

The non-contact inhibited cells at  $\sigma_b/\sigma_f = 1.25$  do not form colonies, instead moving around in a disordered fashion, with a vanishing order parameter. At  $\sigma_b/\sigma_f = 0.80$ , the cells show some alignment, especially at intermediate densities, but are always more weakly aligned than corresponding CIL cells. At  $\sigma_b/\sigma_f = 0.44$ , the cells achieve near perfect orientational order at all densities, just as the CIL cells.

Both CIL and no-CIL cells undergo a dynamical phase transition from disorder to coherent migration, driven by the shape asymmetry of the cells. Thus the shape of the cells acts as an effective alignment mechanism. This transition is very similar to the one found by Wensink et al. [10], where the self-assembly of roughly triangular, stiff, active particles was investigated, but we find the transition to be *reversed*: cells with a big front travel coherently here and cluster in [10], while cells with a small front cluster here and travel coherently in [10]. The most notable difference between our models and likely the reason behind the reversal of the transition is that cells are highly deformable: they are easily compressed during collisions, which changes the collision dynamics strongly. Cells with small fronts cluster here because their motility tends to stay pointed towards the other disks after a collision. This compresses the cells and inhibits them, leading to cells blocking each other. This clustering may seem somewhat similar to what is observed in other active particle systems [10, 37, 38] but here occurs already at very small density and requires that the dynamics be contact inhibited. Further, in other active particle systems, the average speed upon increasing density typically exhibits a step [10, 39, 40], whereas we find that the velocity decreases continuously. Our model suggests that contact inhibition, while not being solely responsible for alignment of crawling cells, tends to enhance it. Furthermore, the observed transition may explain why crawling cells often exhibit a broad front: *It avoids clustering*.

In the transition into arrest at  $\sigma_b/\sigma_f = 0.80$  a remarkable feature develops: areas of dynamic arrest form and dissolve

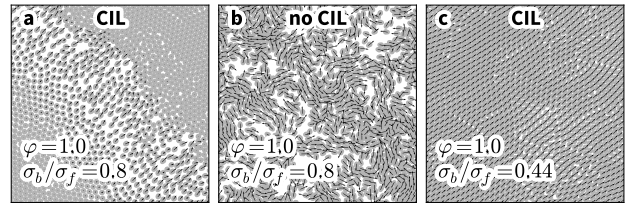


Figure 5. Simulation snapshots of CIL and no-CIL cells in the steady state with the velocity of cells plotted as arrows. (For videos, see supplementary materials)

again. The typical size of these arrested areas grows in size with density until become system-spanning waves of arrest, see fig. 5a). The waves travel against the direction of motion of the cells, akin to traffic jams in models for car traffic [41–43]. The growth of the waves suggests the presence of a diverging length scale. The onset of system-spanning arrest waves roughly coincides with the decrease of the order parameter for  $\varphi \approx 0.85$ . We don't observe such waves in the non-CIL systems, see fig. 5b), thus directly connecting the waves to the contact inhibition mechanism. Intriguingly, the cells with shape asymmetry  $\sigma_b/\sigma_f = 0.44$ , exhibit slowing down but no traffic jams. Instead, the cells always travel coherently, fig. 5c). The reason for this lies in the cell shape: When cells collide, they are compressed. If the size asymmetry is more extreme, it means that the distance  $r_{bf}$  between the disk centers in the most compressed state tends to be bigger. Since the motility force is proportional to  $r_{bf}$ , more asymmetric cells are automatically less inhibited and their slowing down is less pronounced. This restraint in breaking can suppress jams in traffic models and thus explains the qualitative difference between the two systems.

**Summary** In order to reveal universal dynamics of contact inhibited, deformable cells, we modelled crawling cells on a substrate in a minimal, mechanical model. Cell motility was motivated by the internal dynamics of the cells. We assumed the motility force to be proportional to the extension of the cell, thus giving rise to contact inhibition of locomotion naturally. We find rich dynamic behavior with multiple phase transitions as a function of cell shape, cell density and whether locomotion is inhibited or not. Our results may explain why migrating cells often exhibit a broad front: It avoids clustering.

This system is a natural candidate to further investigate the dynamics of cellular tissues. In particular, we expect insights from investigating the effect of contact inhibition and cell shape on tissue growth and wound closure. In addition, the dynamics of malignant cells can be investigated in mixtures of contact-inhibited and non-contact-inhibited cells.

**Acknowledgements** We thank Norihiro Oyama, Mitsusuke Tarama and Jürgen Horbach for helpful discussions. This work was supported by the Japan Society for the Promotion of Science (JSPS) KAKENHI Grant No. 26247069 and 26610131. We also acknowledge the supporting program for

interaction-based initiative team studies (SPIRITS) of Kyoto University.

\* skschnyder@gmail.com

- [1] D. J. Montell, *Science* **322**, 1502 (2008).
- [2] P. Friedl and D. Gilmour, *Nat. Rev. Mol. Cell Biol.* **10**, 445 (2009).
- [3] P. Rørth, *Annu. Rev. Cell Dev. Biol.* **25**, 407 (2009).
- [4] J. H. Kim, X. Serra-Picamal, D. T. Tambe, E. H. Zhou, C. Y. Park, M. Sadati, J.-A. Park, R. Krishnan, B. Gweon, E. Millet, et al., *Nat. Mater.* **12**, 856 (2013).
- [5] Y. T. Maeda, J. Inose, M. Y. Matsuo, S. Iwaya, and M. Sano, *PLoS One* **3** (2008).
- [6] K. Keren, Z. Pincus, G. M. Allen, E. L. Barnhart, G. Marriott, A. Mogilner, and J. A. Theriot, *Nature* **453**, 475 (2008).
- [7] F. Ziebert, S. Swaminathan, and I. S. Aranson, *J. R. Soc. Interface* **9**, 1084 (2012).
- [8] T. Ohta, M. Tarama, and M. Sano, *Phys. D* **318-319**, 3 (2015), 1509.05215.
- [9] V. Kantsler, J. Dunkel, M. Polin, and R. E. Goldstein, *Proc Natl Acad Sci U S A* **110**, 1187 (2013), arXiv:1301.4099v1.
- [10] H. H. Wensink, V. Kantsler, R. E. Goldstein, and J. Dunkel, *Phys. Rev. E - Stat. Nonlinear, Soft Matter Phys.* **89**, 1 (2014), 1306.0709.
- [11] D. Grossman, I. S. Aranson, and E. Ben Jacob, *New J. Phys.* **10**, 1 (2008).
- [12] L. Coburn, L. Cerone, C. Torney, I. D. Couzin, and Z. Neufeld, *Phys. Biol.* **10**, 046002 (2013).
- [13] T. Ohta and S. Yamanaka, *Eur. Phys. J. Spec. Top.* **223**, 1279 (2014), 1403.6567.
- [14] J. Löber, F. Ziebert, and I. S. Aranson, *Sci. Rep.* **5**, 9172 (2015).
- [15] M. Abercrombie, *Nature* **281**, 259 (1979).
- [16] E. Theveneau and R. Mayor, *Small GTPases* **1**, 113 (2010).
- [17] C. Carmona-Fontaine, E. Theveneau, A. Tzekou, M. Tada, M. Woods, K. M. Page, M. Parsons, J. D. Lambris, and R. Mayor, *Dev. Cell* **21**, 1026 (2011).
- [18] A. Puliafito, L. Hufnagel, P. Neveu, S. Streichan, A. Sigal, D. K. Fygenson, and B. I. Shraiman, *Proc. Natl. Acad. Sci.* **109**, 739 (2012).
- [19] R. Mayor and C. Carmona-Fontaine, *Trends Cell Biol.* **20**, 319 (2010).
- [20] E. Theveneau, L. Marchant, S. Kuriyama, M. Gull, B. Moepps, M. Parsons, and R. Mayor, *Dev. Cell* **19**, 39 (2010).
- [21] J. Zimmermann, B. A. Camley, W.-J. Rappel, and H. Levine, *Proc. Natl. Acad. Sci.* **113** (2016).
- [22] J. F. Li and J. Lowengrub, *J. Theor. Biol.* **343**, 79 (2014).
- [23] D. A. Lauffenburger and A. F. Horwitz, *Cell* **84**, 359 (1996).
- [24] A. J. Ridley, M. A. Schwartz, K. Burridge, R. A. Firtel, M. H. Ginsberg, G. Borisy, J. T. Parsons, and A. R. Horwitz, *Science* **302**, 1704 (2003).
- [25] R. Ananthakrishnan and A. Ehrlicher, *Int. J. Biol. Sci.* **3**, 303 (2007).
- [26] S. Vedel, S. Tay, D. M. Johnston, H. Bruus, and S. R. Quake, *Proc. Natl. Acad. Sci. U. S. A.* **110**, 129 (2013).
- [27] A. Mogilner and K. Keren, *Curr. Biol.* **19**, R762 (2009).
- [28] S. Jin and L. R. Collins, *New J. Phys.* **9** (2007).
- [29] K. Drescher, J. Dunkel, L. H. Cisneros, S. Ganguly, and R. E. Goldstein, *Proc. Natl. Acad. Sci.* **108**, 10940 (2011).
- [30] H. H. Wensink, J. Dunkel, S. Heidenreich, K. Drescher, R. E. Goldstein, H. Lowen, and J. M. Yeomans, *Proc. Natl. Acad. Sci.* **109**, 14308 (2012), 1208.4239v1.
- [31] W. J. Nelson, *Cold Spring Harb. Perspect. Biol.* **1**, 1 (2009).
- [32] J. Weeks, D. Chandler, and H. C. Andersen, *J. Chem. Phys.* **54**, 5237 (1971).
- [33] T. Vicsek, A. Czirók, E. Ben-Jacob, I. Cohen, and O. Shochet, *Phys. Rev. Lett.* **75**, 1226 (1995).
- [34] G. Grégoire and H. Chaté, *Phys. Rev. Lett.* **92**, 025702 (2004), 0401208.
- [35] H. Chaté, F. Ginelli, G. Grégoire, and F. Raynaud, *Phys. Rev. E* **77**, 046113 (2008).
- [36] C. Carmona-Fontaine, H. K. Matthews, S. Kuriyama, M. Moreno, G. A. Dunn, M. Parsons, C. D. Stern, and R. Mayor, *Nature* **456**, 957 (2008).
- [37] I. Buttinoni, J. Bialké, F. Kümmel, H. Löwen, C. Bechinger, and T. Speck, *Phys. Rev. Lett.* **110**, 238301 (2013), 1305.4185.
- [38] C. Bechinger, R. Di Leonardo, H. Löwen, C. Reichhardt, G. Volpe, and G. Volpe, pp. 1–54 (2016), arXiv:1602.00081v1.
- [39] F. D. C. Farrell, O. Hallatschek, D. Marenduzzo, and B. Walclaw, *Phys. Rev. Lett.* **111**, 168101 (2013).
- [40] G. S. Redner, M. F. Hagan, and A. Baskaran, *Phys. Rev. Lett.* **110**, 1 (2013), 1207.1737.
- [41] A. S. De Wijn, D. M. Miedema, B. Nienhuis, and P. Schall, *Phys. Rev. Lett.* **109**, 1 (2012), 1205.6486.
- [42] K. Nagel and M. Schreckenberg, *J. Phys. I* **2**, 2221 (1992).
- [43] D. Helbing, *Rev. Mod. Phys.* **73**, 1067 (2001), 0012229.